ISSN 0023-1584, Kinetics and Catalysis, 2006, Vol. 47, No. 4, pp. 585–592. © MAIK "Nauka/Interperiodica" (Russia), 2006.
Original Russian Text © A.N. Il'ichev, A.A. Firsova, V.N. Korchak, 2006, published in Kinetika i Kataliz, 2006, Vol. 47, No. 4, pp. 602–609.

Mechanism of CO Oxidation in Excess H_2 over CuO/CeO_2 Catalysts: ESR and TPD Studies

A. N. Il'ichev, A. A. Firsova, and V. N. Korchak

Semenov Institute of Chemical Physics, Russian Academy of Sciences, Moscow, 117977 Russia

Received December 6, 2004

Abstract—The oxidation of CO with oxygen over (0.25–6.4)% CuO/CeO_2 catalysts in excess H_2 is studied. CO conversion increases and the temperature range of the reaction decreases by 100 K as the CuO content is raised. The maximal CO conversion, 98.5%, is achieved on 6.4% CuO/CeO_2 at 150°C. At $T > 150$°C, the CO conversion decreases as a result of the deactivation of part of the active sites because of the dissociative adsorption of hydrogen. CO is efficiently adsorbed on the oxidized catalyst to form CO–Cu^+ carbonyls on Cu_2O clusters and is oxidized by the oxygen of these clusters, whereas it is neither adsorbed nor oxidized on Cu^0 of the reduced catalysts. The activity of the catalysts is recovered after the dissociative adsorption of O_2 on Cu^0 at $T \sim$ 150°C. The activation energies of CO, CO_2, and H_2O desorption are estimated, and the activation energy of CO adsorption yielding CO–Cu^+ carbonyls is calculated in the framework of the Langmuir–Hinshelwood model.

DOI: 10.1134/S002315840604015X

INTRODUCTION

The low-temperature heterogeneous oxidation of CO with oxygen in excess hydrogen is a promising reaction for efficient fuel cells [1]. A survey of catalysts for CO oxidation shows that the oxide system CuO–CeO_2 is one order of magnitude more active than platinum group metals supported on Al_2O_3 or zeolites [2–4]. The mechanism of this reaction on CuO–CeO_2 and CuO–CeO_2–ZrO_2 systems is being actively debated [5, 6], and new catalysts are being sought for this reaction [7–11].

The high activity of CuO–CeO_2 catalysts in low-temperature CO oxidation is due to the synergistic effect arising from the Cu–Ce interaction, which facilitates the reduction and oxidation of both components. The formation of the radical anion O_2^- during the adsorption of CO + O_2 at room temperature is believed to be evidence of this synergism. However, the O_2^-(CO + O_2) species has recently been found on pure oxidized CeO_2 [12, 13], in the absence of a synergistic effect. In this connection, it is of interest to obtain further evidence of the synergistic effect in CuO–CeO_2 by investigating the formation of O_2^- during the adsorption of CO + O_2 on CuO/CeO_2 samples with various CuO contents.

Here, we report the catalytic activity of CeO_2 and (0.25–6.4)% CuO/CeO_2 as a function of CuO content for CO oxidation with oxygen in excess hydrogen in the temperature range 100–350°C. In order to elucidate the nature of the active sites and intermediates, the adsorption of CO, O_2, H_2, and their mixtures on oxidized and reduced (0.25–6.4)% CuO/CeO_2 catalysts was studied by ESR and TPD in the temperature range 20–200°C.

EXPERIMENTAL

Ceria with a specific surface area of $S_{sp} = 73$ m^2/g was prepared by the decomposition of $Ce(NO_3)_4 \cdot 6H_2O$ in air at 500°C for 2 h. The specific surface area was determined by the BET method from low-temperature argon adsorption data.

CuO/CeO_2 samples containing 0.25, 0.5, 1.0, 2.1, and 6.4 wt % CuO were prepared by impregnating CeO_2 with copper nitrate solutions with various salt concentrations followed by drying at 100°C and calcination in air at 500°C for 2 h. The specific surface area of the samples decreases from 73 to 63 m^2/g as the CuO content is raised from 0.25 to 6.4%. The ratio of the number of copper ions to the number of surface cerium ions was varied from 0.1 to 2.1 under the assumption that copper ions are uniformly distributed on the CeO_2 surface.

The catalytic activity of the samples in CO oxidation with oxygen in excess hydrogen was studied in a flow reactor. A catalyst sample (20 mg) was charged into a quartz reactor (tube 3 mm in diameter), and the reactor was purged with the reaction mixture (98 vol % H_2 + 1 vol % CO + 1 vol % O_2) at a flow rate of 40 ml/min. The reaction products were analyzed using two columns packed with the molecular sieve NaX (13 Å) and Porapak QS, respectively. Thermal conductivity detectors were used.

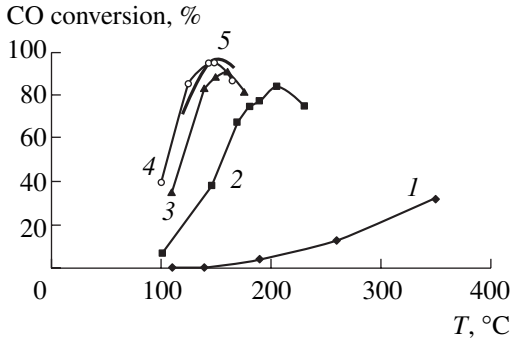

Fig. 1. Catalytic activity of CuO/CeO_2 samples in CO oxidation with oxygen in excess hydrogen. CuO content: (*1*) 0, (*2*) 0.5, (*3*) 1.0, (*4*) 2.1 and (*5*) 6.4%.

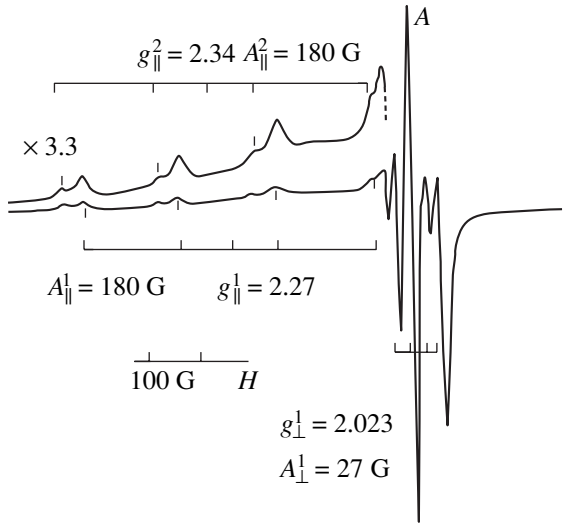

Fig. 2. ESR spectrum of Cu^{2+} in the 0.25% CuO/CeO_2 (O_2, 500°C) in a vacuum at –196°C.

The state of copper ions in the oxidized and reduced samples (0.25–6.4)% CuO/CeO_2 was studied by ESR. A 50-mg sample was placed into an ESR ampoule, pumped to 10^{-4} Pa, heated *in vacuo* at 500°C for 1 h, and then oxidized with O_2 ($P = 2 \times 10^2$ Pa) or reduced with H_2 ($P = 1 \times 10^3$ Pa) at this temperature for 20 min. After oxidation, the sample was cooled to 20°C in O_2 and pumped. In the case of reduction, the sample was pumped at 500°C for 15 min and then cooled to room temperature. ESR spectra were recorded at –196 and 20°C in the X-band region on an ESR-V spectrometer with a Diapazon temperature attachment. The amount of paramagnetic species was determined from the ESR spectra after double integration and comparison with the reference sample, $CuSO_4 \cdot H_2O$. The accuracy of these measurements was 20%.

The CO adsorption species and their interaction with O_2 and H_2 on CeO_2 and (0.25–6.4)% CuO/CeO_2 were studied by vacuum TPD. A 50-mg sample was preliminarily oxidized or reduced at 500°C, and then a gas was adsorbed at 20°C. After adsorption, the gas was pumped out and the sample was heated at a rate of 10 K/min under continuous pumping. TPD spectra as the change in the pressure of desorbed gas (W) as a function of temperature (T) were obtained using a Pirani manometer [14]. The composition of desorbed gas was monitored with an MX-7304 mass-spectrometer. The amount of desorbed gas was estimated in a TPD run conducted in a sealed reactor.

The gases CO, O_2, and H_2 were obtained according to standard procedures [15]. They were admitted to the sample through a liquid nitrogen trap to remove the uncontrolled CO_2 and H_2O impurities.

RESULTS

Catalytic Activity of CuO/CeO_2 in CO Oxidation with Oxygen in Excess Hydrogen

Figure 1 plots CO conversion versus temperature on samples with various CuO contents that were preliminarily heated in air for 1 h. As can be seen in Fig. 1, the CO conversion on CeO_2 is not high, being at most 30% at 350°C. Supporting a small amount of CuO (0.5% CuO/CeO_2 sample) raises the conversion from 5 to 85% in the temperature range from 100 to 200°C. The conversion is maximal at $T_{max} = 200$°C and decreases to 75% as the temperature is further increased to 220°C. An extremum in the temperature dependence of CO conversion is also observed for the other CuO-containing samples. As the CuO content is increased from 0.5 to 6.4%, the maximal CO conversion changes from 85 to 98.5% and T_{max} decreases from 200 to 150°C. The decrease in CO conversion at $T > T_{max}$ cannot be due to an irreversible poisoning of the catalyst since the initial value of conversion is restored as the reaction temperature is decreased to T_{max}. The maximal CO conversion is 98.5% and is observed for 6.4% CuO/CeO_2.

ESR Data

Isolated Cu^{2+} cations in (0.25–6.4)% CuO/CeO_2. Figure 2 presents the ESR spectrum of Cu^{2+} cations in the oxidized 0.25% CuO/CeO_2 (O_2, 500°C) sample recorded at –196°C. This spectrum is typical of isolated Cu^{2+} cations in both zeolites [16, 17] and CeO_2 [18]. The spectrum consists of axially symmetric signals with $g_{\perp} > g_{\parallel} > g_e$. The HFS lines are due to the interaction between unpaired electrons with the nuclear spin $I = 3/2$. Two signals can be distinguished here. Signal 1 is characterized by $g_{\perp}^1 = 2.023$, $A_{\perp}^1 = 27$ G, $g_{\parallel}^1 = 2.27$, and $A_{\parallel}^1 = 180$ G; signal 2, by $g_{\parallel}^2 = 2.34$, and $A_{\parallel}^2 \sim 180$ G. The lines of signal 2 likely overlap with the lines of signal 1 in the high-field region. This allows one to

assume that $g_{\perp}^1 \sim g_{\perp}^2$ and $A_{\parallel}^1 \sim A_{\parallel}^2$. The main contribution to the ESR spectrum is from signal 1. The total concentration of paramagnetic Cu^{2+} cations in 0.25% CuO/CeO_2 is 1.3×10^{17} m^{-2}, ~30% of the concentration of supported copper ions.

The ESR spectra of Cu^{2+} in the (0.5–6.4)% CuO/CeO_2 samples (O_2, 500°C) are similar to the spectrum presented in Fig. 2. Figure 3 plots the relative intensity ($J_{rel} = J/J_{max}$) of line *A* in the ESR spectrum of Cu^{2+} versus the CuO content of CeO_2. The intensity of this line decreases by a factor of 15 as the CuO content of CeO_2 increases from 0.25 to 6.4%. The other lines of the spectrum change in a similar way. This is evidence of a decrease in the proportion of isolated Cu^{2+} cations in CeO_2.

Thus, isolated Cu^{2+} ions are present in (0.5–6.4)% CuO/CeO_2 (O_2, 500°C), and their concentration decreases with an increase in the copper content of CeO_2. Isolated Cu^{2+} cations in CeO_2 likely form oxo complexes with two different coordination spheres. The *g*-tensors of these signals are in agreement with those of Cu^{2+} in various oxide systems, in which the coordination sphere of copper cations varies from distorted octahedral to pyramidal and square-planar [18]. In this connection, note that the parameters of the ESR spectrum of Cu^{2+} in CuO/CeO_2 ($g_{\perp}^1 = g_{\perp}^2 = 2.023$, $A_{\perp}^1 = A_{\perp}^2 =$ 27 G, $g_{\parallel}^2 = 2.34$, $A_{\parallel}^2$ ~180 G, $g_{\parallel}^1 = 2.27$, and $A_{\parallel}^1 =$ 180 G) are close to those for Cu^{2+} cations in CuZSM-5, which have a square-pyramidal or square-planar coordination sphere [16]. Further investigation is required for a more detailed consideration of this point.

Formation of O_2^- during adsorption of CO + O_2 and O_2 on (0.25–6.4)% CuO/CeO_2. Upon the admission of CO or O_2 ($P = 2 \times 10^2$ Pa, 20°C) to the oxidized (0.25–6.4)% CuO/CeO_2 (O_2, 500°C) samples, the ESR signal of Cu^{2+} does not change in the case of CO and broadens in the case of O_2. However, after CO adsorption for 1–2 min followed by removal of the gas and admission of O_2, a new signal appears in the ESR spectrum. Its intensity decreases by 1/4 upon pumping the sample at 20°C for 1 h. The signal disappears upon holding the sample at 100°C *in vacuo* for 10 min. Only a signal from isolated Cu^{2+} cations remains in the ESR spectrum. Its intensity is equal to the intensity of the signal from Cu^{2+} in the initial sample. Figure 4 presents the Cu^{2+} ESR spectrum in the region of $g_{\perp}$ values for the sample 0.25% CuO/CeO_2 (O_2, 500°C) *in vacuo* at 20°C (spectrum *1*), the ESR spectrum recorded after the adsorption of CO + O_2 on the same catalyst (O_2, 500°C) (spectrum *2*), and their difference (spectrum *3*). Spectrum *3* is complicated and shows an anisotropic signal with $g^1 = 2.047$, $g^2 = 2.034$, and $g^3 = 2.009$. The shape, thermal behavior, and the *g*-tensor of the spectrum are

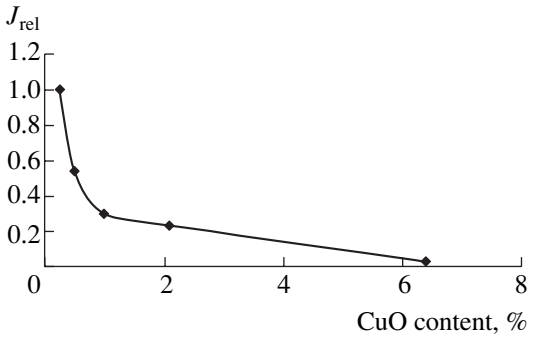

Fig. 3. Intensity of line *A* in the ESR spectrum of Cu^{2+} (see Fig. 2) versus the CuO content of CeO_2.

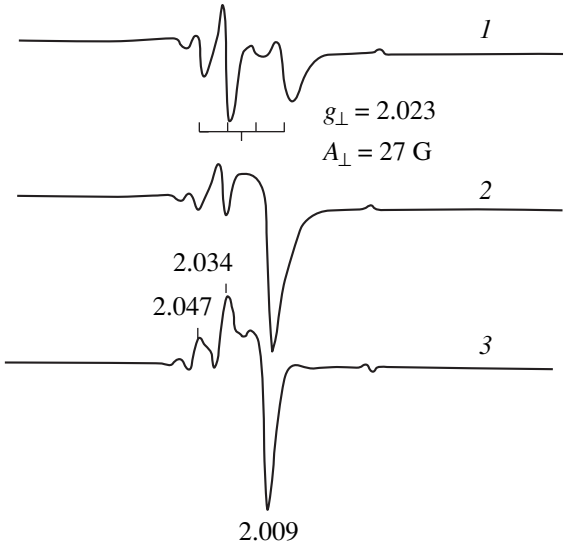

Fig. 4. (*1*) Cu^{2+} ESR spectrum in the $g_{\perp}$ region for 0.25% CuO/CeO_2 (O_2, 500°C) in a vacuum at 20°C, (*2*) the same spectrum after the adsorption of CO + O_2, and (*3*) the difference spectrum.

characteristic of the O_2^- radical anion. This species results from the reaction CO + O_2 on oxidized CeO_2 [13] or from O_2 adsorption on CeO_2 preliminarily reduced *in vacuo* at $T = 400$°C [13, 19] and is stabilized in the coordination sphere of Ce^{4+} cations in various anionic vacancies. Based on our earlier study of the temperature dependence of the ESR spectrum of O_2^- [13], we believe that spectrum *3* consists of at least two anisotropic signals, whose lines are separated in the g_{zz} range from 2.055 to 2.016 and are greatly overlapped at g_{xx} and g_{yy} of 2.016 to 2.003 at 20°C. The line with $g_{zz}^1 = 2.047$ is evidence of the stabilization of O_2^- on associated anionic vacancies, whereas the line with $g_{zz}^2 = 2.034$ points to the stabilization of O_2^- in isolated anionic vacancies. The concentration of radical anions

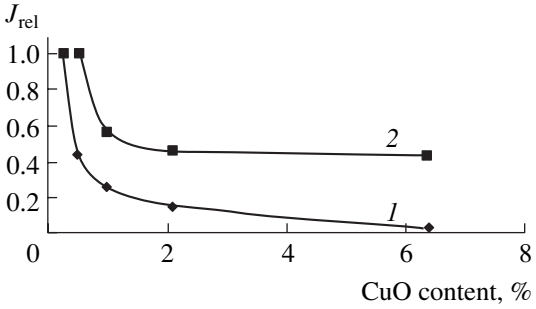

Fig. 5. Relative intensity of the O_2^- signal versus CuO content for (*1*) CuO/CeO_2 (O_2, 500°C) samples after the adsorption of CO + O_2 and (*2*) CuO/CeO_2 (H_2, 500°C) samples after O_2 adsorption.

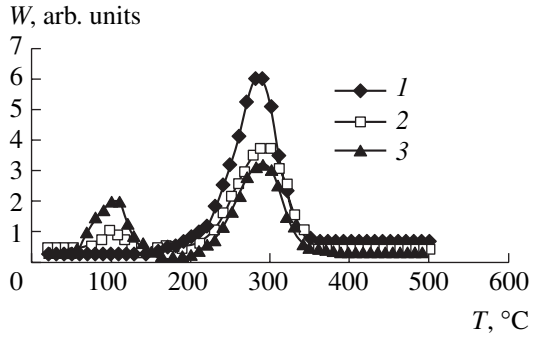

Fig. 6. TPD spectra for CuO/CeO_2 (H_2, 500°C) samples after CO adsorption at 20°C. CuO content: (*1*) 0, (*2*) 0.5, and (*3*) 6.4%.

on the 0.25% CuO/CeO_2 (O_2, 500°C) surface is 5.0×10^{16} m^{-2} and is close to their concentration on pure CeO_2.

The dependence of the relative intensity (J_{rel}) of the ESR line of $O_2^-(CO + O_2)$ on the CuO content for the oxidized samples (Fig. 5, curve *1*) shows that the amount of O_2^- decreases monotonously to zero as the CuO content is increased from 0.25 to 6.4%. Hence, the copper ion suppresses the formation of $O_2^-(CO + O_2)$ on the oxidized CeO_2 surface.

The Cu^{2+} ESR signal from the reduced (0.25–6.4)% CuO/CeO_2 (H_2, 500°C) samples is 20–30 times weaker than the same signal from the oxidized samples. However, the radical anion O_2^- ($g^1 = 2.047$, $g^2 = 2.034$, $g^3 = 2.009$) results from the adsorption of oxygen ($P = 2 \times 10^2$ Pa, 20°C) on the reduced samples, and their concentration, $(1.5–3.0) \times 10^{17}$ m^{-2}, is higher than the $O_2^-(CO + O_2)$ concentration on the oxidized samples. As can be seen in Fig. 5 (curve *2*), the amount of O_2^- in this case decreases only by a factor of 2 as the CuO content increases from 0.25 to 6.4%.

For the radical anion O_2^-, $g_{xx} \sim 2.009$ is higher than $g_e = 2.0023$, indicating the formation of a covalent bond due to the overlap of the occupied π_y-orbital of oxygen with the unoccupied 4*f* orbital of the Ce^{4+} cation [12]. The covalent bond in this complex is less strong than the ionic bond in $O_2^-Zr^{4+}$ [20]. The presence of several kinds of O_2^- species and their different thermal stability are likely due to their stabilization on cerium cations with different coordination spheres. The possibility of O_2^- radical anions ($g_{zz} = 2.030$) being stabilized on CeO_2 anions was mentioned in an earlier work [12].

TPD Data

CO and CO_2 adsorption species on (0.25–6.4)% CuO/CeO_2. As can be seen in Fig. 6, the TPD spectra of reduced CeO_2 and (0.5, 6.4)% CuO/CeO_2 (H_2, 500°C) contain a peak at $T_{max} \approx 300$°C after adsorption of CO ($P = 2 \times 10^2$ Pa, $T = 20$°C, $t = 10$ min). The intensity of the peak is maximal for CeO_2. The amount of desorbed CO per unit surface area is 1.0×10^{17} m^{-2}. As the copper content of the sample is increased from 0.5 to 6.4%, the amount of desorbed CO is halved (spectra *1*, *3*). The presence of a CO peak at 300°C in the TPD spectra of CeO_2 and (0.5–6.4)% CuO/CeO_2 is evidence that CO desorbs from the surface of the CeO_2 support of the copper-containing samples and does not adsorb on reduced copper, which is likely to be in the Cu^0 state.

It is also evident from Fig. 6 that a small amount of CO desorbs from CuO/CeO_2 at ~100°C. This is likely due to the decomposition of the surface complexes formed by adsorbed CO and copper cations.

After CO adsorption ($P = 2 \times 10^2$ Pa, $T = 20$°C, $t =$ 10 min) on oxidized CeO_2 and (0.25–6.4)% CuO/CeO_2 (O_2, 500°C), gas desorption from CeO_2 is negligible as compared to desorption from the copper-containing samples. Several H_2 desorption peaks are observed in the TPD spectra of the copper-containing samples. As can be seen in Fig. 7, the peaks at 100 and 160°C in the low-temperature range of the spectrum grow with an increase in the CuO content from 0.25 to 6.4%. At higher temperatures, the maximum of the broad peak shifts from 450 to 270°C. CO is desorbed in the low-temperature range of the spectrum, whereas CO_2 is desorbed at higher temperatures. In the case of 6.4% CuO/CeO_2 (O_2, 500°C), the CO and CO_2 desorption peaks are overlapped to a considerable extent, but they can still be separated from one another. Figure 8 presents the TPD spectra recorded after CO adsorption on 6.4% CuO/CeO_2 (O_2, 500°C). Spectrum *1* is the superposition of the CO and CO_2 desorption spectra. Spectrum *2* corresponds to the desorption of CO alone. This spectrum was recorded upon CO_2 freezing in a liquid nitrogen trap placed at the outlet of the reactor before

the Pirani manometer. Spectrum *3* is the difference between spectra *1* and *2* and characterizes CO_2 desorption. Spectrum *2* has a maximum at $T_{max} = 100°C$ and a shoulder at ~150°C. In this temperature range, CO desorption is due to the decomposition of CO–Cu^+ carbonyls of two types, in which copper cations have different coordination spheres [5]. Their concentration is 8×10^{17} m^{-2}. Spectrum *3* is complicated, with the CO_2 desorption rate peaking at 150 and 250°C. The desorption peak at 150°C is likely due to the oxidation of adsorbed CO with surface oxygen, since the maximal CO conversion on this sample is observed at this temperature (see Fig. 1). The broad peak at 250°C is possibly due to the slow decomposition of surface carbonates [5]. The concentrations of desorbed CO_2 calculated from spectrum *3* and from the amount of CO_2 frozen in the liquid nitrogen trap in the TPD run are similar, being 1.2×10^{18} and 1.7×10^{18} m^{-2}, respectively.

In a TPD run carried out after CO adsorption on the 6.4% CuO/CeO_2 sample not oxidized with oxygen, the amounts of desorbed CO and CO_2 were half as large. After two successive runs, these amounts were smaller by a factor of 5. Heating the sample in oxygen at $T \geq 150°C$ for 10 min resulted in the complete recovery of catalytic activity.

Thus, as the CuO content of CeO_2 in the oxidized samples increases, both CO adsorption and the amount of CO oxidized with surface oxygen increase and the CO_2 desorption temperature decreases. The surface oxygen consumed in oxidation is recovered upon heating the sample in O_2 at 150°C.

Effect of oxygen adsorption on CO_2 desorption. Figure 9 presents the TPD spectra for 6.4% CuO/CeO_2 (O_2, 500°C) after CO adsorption ($P = 2 \times 10^2$ Pa, $T =$ 20°C, $t = 10$ min) (spectrum *1*) and after oxygen adsorption ($P = 2 \times 10^2$ Pa, $T = 20°C$, $t = 5$ min) on a pumped sample containing preliminarily adsorbed CO (spectrum *2*). The broad CO_2 desorption peak in the 200–450°C range in spectrum *1* is stronger than the same peak in spectrum *2*. In the former case, the concentration of desorbed molecules is 2.5×10^{18} m^{-2}; in the latter case, this concentration is 2.1×10^{18} m^{-2}. The difference is 4.0×10^{17} m^{-2}. It was found that, as O_2 is adsorbed, CO_2 desorbs from the surface. The amount of desorbed CO_2 frozen in the liquid nitrogen trap suggests a value of 4.3×10^{17} m^{-2}, which is equal to the above difference. Lengthening the O_2 adsorption time from 5 min to 1 h increases the amount of desorbed CO_2 only to 5.0×10^{17} m^{-2}. Hence, part of the strongly adsorbed CO_2 is replaced from the surface by oxygen at 20°C.

As shown above, the decrease in the CO conversion at $T > T_{max}$ is not caused by an irreversible poisoning of the catalyst and can be due to the effect of H_2 adsorption on CO adsorption. This point was investigated in greater detail.

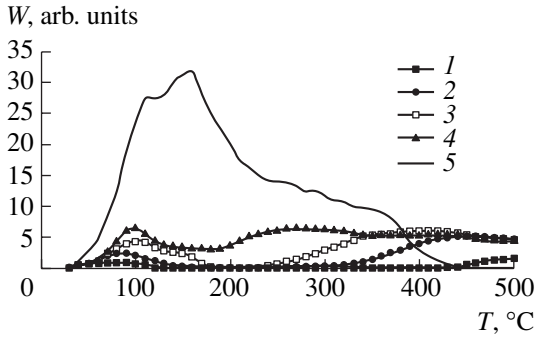

Fig. 7. TPD spectra for CuO/CeO_2 (O_2, 500°C) samples after CO adsorption. CuO content: (*1*) 0.25, (*2*) 0.5, (*3*) 1.0, (*4*) 2.1, and (*5*) 6.4%.

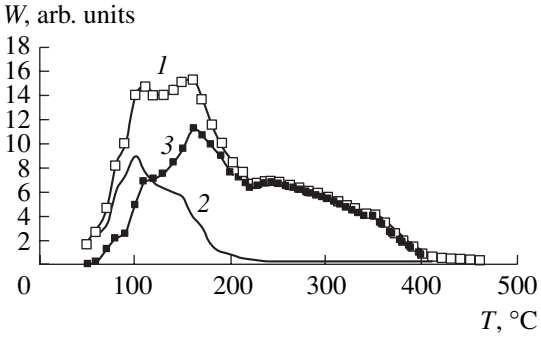

Fig. 8. TPD spectra of the sample 6.4% CuO/CeO_2 (O_2, 500°C) after CO adsorption: (*1*) CO + CO_2, (*2*) CO, and (*3*) CO_2.

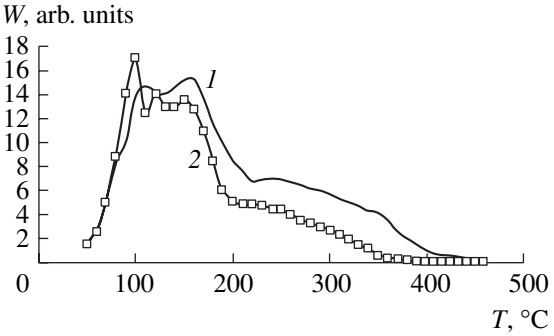

Fig. 9. TPD spectra of the sample 6.4% CuO/CeO_2 (O_2, 500°C) after the adsorption of (*1*) CO and (*2*) CO + O_2.

Effect of adsorbed H_2 on CO adsorption on 6.4% CuO/CeO_2. The effect of adsorbed H_2 on CO adsorption was studied as follows. Initially, H_2 was adsorbed on 6.4% CuO/CeO_2 (O_2, 500°C) ($P = 4 \times 10^2$ Pa, $t =$ 10 min) at a chosen temperature T_{H_2}. After H_2 adsorption, the sample was pumped and cooled to room temperature, CO was adsorbed ($P = 2 \times 10^2$ Pa, $t = 10$ min), and a TPD run was performed. TPD spectra for various

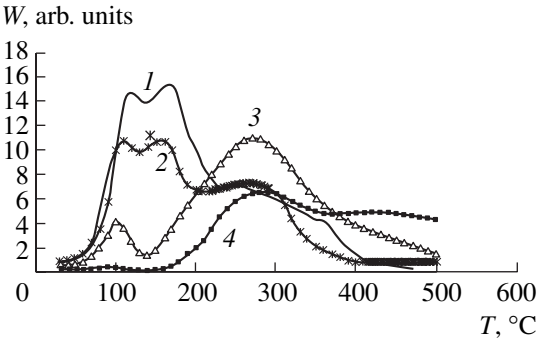

Fig. 10. TPD spectra recorded after CO adsorption on (*1*) 6.4% CuO/CeO_2 (O_2, 500°C) and (*2–4*) 6.4% CuO/CeO_2 (O_2, 500°C) containing H_2 adsorbed at (*2*) 100, (*3*) 160 and (*4*) 200°C.

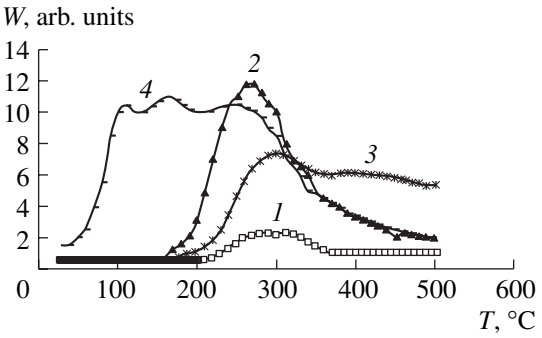

Fig. 11. H_2O TPD spectra of the sample 6.4% CuO/CeO_2 (O_2, 500°C) after H_2 adsorption at (*1*) 100, (*2*) 160, and (*3*) 200°C. (*4*) TPD spectrum of the sample 6.4% CuO/CeO_2 (O_2, 500°C) recorded after the adsorption of H_2 and, thereafter, O_2 at 160°C and CO at 20°C.

T_{H_2} values are presented in Fig. 10. For T_{H_2} = 100°C, the intensities of the CO and CO_2 desorption peaks around 100 and 150°C are 25% lower than the intensity of the TPD peaks measured after CO adsorption on the sample not treated with hydrogen (spectra *1*, *2*). For T_{H_2} = 160°C, the peak at 100°C is 4 times weaker and the peak at 160°C is not observed (spectrum *3*). For T_{H_2} = 200°C, neither peak is observed (spectrum *4*). At the same time, the intensity of the TPD peak at T_{max} ~ 270°C increases as T_{H_2} is raised from 100 to 160°C (spectra *2*, *3*) and then drops at T_{H_2} = 200°C. The changes in the intensity of the desorption peak near 270°C are due to H_2O desorption after hydrogen adsorption. Indeed, as can be seen in Fig. 11, after H_2 adsorption on 6.4% CuO/CeO_2 (O_2, 500°C) at 100, 160, and 200°C for 5 min, only the H_2O desorption peak at 270–300°C is observed in the TPD spectra. Its intensity increases by a factor of ~10 as the hydrogen adsorption temperature is raised from 100 to 160°C (spectra *1*, *2*). At 200°C, its intensity is halved and a broad H_2O desorption peak appears at 400°C (spectrum *3*).

The TPD spectrum of the 6.4% CuO/CeO_2 (O_2, 500°C) sample on which H_2 was adsorbed at 160°C and O_2 was then adsorbed at 160°C for 5 min coincides with spectrum *2*. After CO adsorption at 20°C on 6.4% CuO/CeO_2 (O_2, 500°C) containing H_2 and O_2 adsorbed in sequence at 160°C, the TPD spectrum shows an H_2O desorption peaks at 270°C, which is equal in intensity to the H_2O peak in spectrum *2*, and CO and CO_2 desorption peaks at 100 and 150°C (spectrum *4*). Their intensities are comparable with the intensities of the CO and CO_2 peaks in the TPD spectrum of the oxidized sample after CO adsorption.

Hence, H_2 adsorption at 100–200°C deactivates the CO adsorption and oxidation sites. It is likely that hydrogen is adsorbed dissociatively, is stabilized on oxygen ions, and desorbs from the surface as H_2O at 270–300°C. The active sites are regenerated upon heat treatment in oxygen at 160°C, which does not affect the hydrogen coverage of the surface.

DISCUSSION

As the CuO content of CeO_2 is changed from 0 to 6.4%, CO conversion increases from 30 to 98.5%, accompanied by a decrease in T_{max} from 350 to 150°C (Fig. 1), indicating that the reaction occurs on supported CuO.

Depending on treatment conditions, copper in the catalysts is in the Cu^{2+}, Cu^+, or Cu^0 state, and these ions participate differently in the reaction. CO is not adsorbed on Cu^0 in the reduced catalysts and is not oxidized (Fig. 6). The amounts of adsorbed and oxidized CO on the oxidized catalysts increase with an increase in the CuO content of CeO_2 (Figs. 7, 8). Hence, the active sites can include Cu^{2+} and Cu^+ cations.

According to ESR data, the Cu^{2+} cations form oxo complexes, likely with a square-pyramidal or square-planar coordination sphere, on the oxidized surface (Fig. 2). It is improbable that they participate in CO oxidation, since CO is not adsorbed on these cations at room temperature. Furthermore, the concentration of Cu^{2+} cations decreases with an increase in the CuO content of CeO_2, whereas the CO conversion increases (see Figs. 1 and 3). This inference was confirmed by quantitative data. The concentration of Cu^{2+} oxo complexes in the most active catalyst 6.4% CuO/CeO_2 (~1.0×10^{16} m^{-2}) is two orders of magnitude lower than the concentration of desorbed CO (1.0×10^{18} m^{-2}) or CO_2 (1.5×10^{18} m^{-2}).

The decrease in the amount of isolated Cu^{2+} oxo complexes caused by an increase in the CuO content of CeO_2 is apparently due to the formation of associated Cu^{2+} oxo complexes on the surface. The increasing CuO content causes an increase in the amount of CO

adsorbed on the Cu^+ cations and in the amount of CO oxidized with surface oxygen (Fig. 7), indicating that the active sites are in these associates (Fig. 8) [5]. The temperature range of the deactivation of the active sites in H_2 (100–200°C, Fig. 10) coincides with the temperature range of the reduction of finely dispersed copper clusters on CeO_2 [21]. The structure of these clusters on nanostructured CuO_x/CeO_2 catalysts has been determined [9]: the Cu^+ cations form either a linear structure similar to that of the Cu_2O compound, in which they have two coordination bonds with oxygen ligands, or a planar triangle, whereas the coordination polyhedron of a Cu^{2+} cation is either a CuO_4 tetrahedron or a heavily distorted CuO_6 octahedron. The Cu^+/Cu^{2+} ratio depends on catalyst activation conditions and varies between 0.35 and 0.05. Assuming that the concentration of Cu^+ is equal to the concentration of CO–Cu^+ carbonyls, one can conclude that the Cu^+/Cu^{2+} ratio in 6.4% CuO/CeO_2 is ~0.3.

Thus, the coincidence of the temperature ranges in which the active sites are deactivated and the copper oxide clusters are reduced with hydrogen, as well as the similarity between the Cu^+/Cu^{2+} ratios in 6.4% CuO/CeO_2 and nanostructured CuO_x/CeO_2, suggests that CO likely adsorbs on the Cu_2O clusters to form CO–Cu^+ carbonyl complexes.

The amount of oxidized CO increases and the CO_2 desorption temperature decreases with an increase in the CuO coverage of the CeO_2 surface (Fig. 7). Therefore, adsorbed CO is oxidized with the oxygen of the Cu_2O clusters, possibly the bridging or terminal oxygen of the Cu^{2+}–O^{2-}–Cu^{2+} or Ce^{4+}–O^{2-}–Cu^{2+} species.

The O_2^- radical anions are stabilized in the coordination sphere of the coordinatively unsaturated Ce^{4+} cations. Their amount is proportional to the surface area of the support that is not occupied by supported copper species. As can be seen in Fig. 5, the copper coverage of the surface in the reduced (2.1–6.4)% CuO/CeO_2 catalysts is at most ~50% (curve *2*), whereas it is close to 100% in the oxidized 6.4% CuO/CeO_2 catalyst. This fact is in agreement with the high degree of dispersion of copper oxide on the CeO_2 surface. The increase in the free surface area of the support upon the reduction of the catalyst is due to the aggregation of Cu^0 atoms into three-dimensional species. The oxidation of copper likely yields two-dimensional association species of copper oxo complexes dispersed on the surface. These structural changes in supported copper occur through the migration of ions and atoms. It was assumed that the copper atoms migrate to anionic vacancies [9]. On the other hand, oxygen adsorbed on anionic vacancies is stabilized as O_2^-. This oxygen species was considered in some studies [5, 6, 22] to be an intermediate in the catalyst reoxidation. However, on the reduced catalyst 6.4% CuO/CeO_2, the O_2^- concentration (1.5×10^{17} m^{-2}) is insufficient for the regeneration of the adsorption and CO oxidation sites, whose concentrations are 0.8×10^{18} and 1.7×10^{18} m^{-2}, respectively. Note that these sites are not regenerated with oxygen at 20°C, but, when the reoxidation temperature is increased to 160°C, their concentration corresponds to the number of active sites in the oxidized catalyst. Apparently, catalyst reoxidation occurs through the dissociative adsorption of O_2 on Cu^0 species, contrary to the opinion that it occurs through O_2^- transformation to ionic species [5, 6, 22].

Hydrogen on the surface of 6.4% CuO/CeO_2 at 100–200°C is stabilized as the hydroxyl species H^+–O^{2-}, as is indicated by the fact that it desorbs as H_2O at 270–300°C (Fig. 11). Hydrogen adsorption decreases the number of CO adsorption and oxidation sites (Fig. 10), because of the reduction of Cu^+ cations to Cu^0 and the formation of hydroxyl groups. Since the temperature range of hydrogen adsorption (100–200°C) overlaps partially with the range in which CO conversion on 6.4% CuO/CeO_2 decreases ($T_{max} > 150$°C), the decrease in catalytic activity is due to the additional deactivation of part of the active sites by adsorbed hydrogen. Note that, after hydrogen adsorption on the surface, the active sites are regenerated by oxygen at 150°C (Fig. 11).

The adsorption of a CO + O_2 mixture on the oxidized CuO/CeO_2catalysts yields O_2^- radical anions on coordinatively unsaturated Ce^{4+} cations. These species do not participate in CO oxidation on CuO/CeO_2, since the rate of $O_2^-(CO + O_2)$ generation drops with increasing CuO content (see Fig. 5), whereas CO conversion increases (Fig. 1). The finding that the $O_2^-(CO + O_2)$ concentration increases monotonically with increasing CuO content of CeO_2 indicates that $O_2^-(CO + O_2)$ formation on CeO_2 is inhibited by copper oxide and there is no additional channel of $O_2^-(CO + O_2)$ generation due to the synergistic effect in this reaction. The inhibiting effect is due to the fact that the free surface area of CeO_2 decreases with increasing CuO coverage. In this case, a decrease in the rate of $O_2^-(CO + O_2)$ formation can be due to either a decrease in the number of O_2^- stabilization sites or a decrease in the number of electron donor complexes (active carboxylates and carbonates) on the CeO_2 surface [12, 13].

As shown above, oxygen is necessary for maintaining the catalyst in the oxidized state active in CO conversion. Furthermore, oxygen adsorption at 20°C stimulates the desorption of part of the CO_2 strongly bound to the surface, which occurs at $T \geq 160$°C in the absence of oxygen (Fig. 8). CO conversion at 20°C [5] is likely due to this replacement effect.

The TPD data presented in Figs. 8 and 11 enable one to estimate the activation energies of CO, CO_2, and H_2O desorption from the equation $E_{des} = 25RT_{max}$ [23]

(where R is the universal gas constant and T_{max} is the desorption peak temperature (K)). For CO desorption, E_{des} = 77 and 87 kJ/mol for T_{max} = 373 and 423 K, respectively; for CO_2, E_{des} = 87 and 107 kJ/mol for T_{max} = 423 and 523 K, respectively (Fig. 8); for H_2O, E_{des} = 117 kJ/mol for T_{max} = 573 K (Fig. 11).

It was suggested that the low-temperature CO oxidation on $CuO–CeO_2$ occurs through the Langmuir–Hinshelwood mechanism [3, 6]. The kinetics of this reaction were studied, and it was found that the activation energy of CO oxidation is 57 kJ/mol and the heat of CO adsorption is 27 kJ/mol. The heat of adsorption and activation energy of CO desorption allow one to estimate the activation energy of CO adsorption from the equation $E_{ads} = E_{des} - Q$. The formation of the two carbonyl species is characterized by E_{ads} = 50 and 60 kJ/mol, respectively.

Thus, when CO is oxidized with oxygen in excess hydrogen on CuO/CeO_2, carbon monoxide adsorbs on Cu_2O clusters to form two types of $CO–Cu^{2+}$ complexes. Part of these complexes decomposes at 100–160°C, and the other part is oxidized with the bridging oxygen of Cu_2O clusters. The resulting CO_2 desorbs into the gas phase at 160 and 250°C. When CO is oxidized, Cu^+ is reduced to Cu^0. The Cu^+ ions are regenerated upon the dissociative adsorption of O_2 on Cu^0. Hydrogen also adsorbs dissociatively on Cu_2O to form hydroxyl groups and desorbs as H_2O at 300°C. The decrease in CO conversion at $T > 150$°C is mainly due to the increase in the number of deactivated CO oxidation sites during H_2 adsorption.

REFERENCES

1. Kahlich, M.J., Gasteiger, H.A., and Behm, R.J., *J. Catal.*, 1997, vol. 171, p. 93.
2. Liu, W. and Flytzani-Stefanopoulos, M., *J. Catal.,* 1995, vol. 153, p. 304.
3. Liu, W. and Flytzani-Stefanopoulos, M., *J. Catal.,* 1995, vol. 153, p. 317.
4. Avgoropoulos, G., Ioannides, T., Matralis, H., Baatista, J., and Hocevar, S., *Catal. Lett.,* 2001, vol. 73, p. 33.
5. Matinez-Arias, A., Fernandez-Garcia, M., Galvez, O., Coronado, J.M., Anderson, J.A., Conesa, J.C., Soria, J., and Munuera, G., *J. Catal.*, 2000, vol. 195, p. 207.
6. Sedmak, G., Hocevar, S., and Levec, J., *J. Catal.,* 2003, vol. 213, p. 135.
7. Dow, W.-P., Wang, Y.-P., and Huang, T.-G., *Appl. Catal., A*, 2000, vol. 244 (1), p. 155.
8. Avgoropoulos, G. and Ioannides, T., *Appl. Catal., A*, 2003, vol. 190, p. 25.
9. Skarman, B., Grandjean, D., Benfield, R.E., Hinz, A., Andersson, A., and Wallenberg, L.R., *J. Catal.,* 2002, vol. 211, p. 119.
10. Ozkara, S. and Aksoylu, A.E., *Appl. Catal., A,* 2003, vol. 251, p. 75.
11. Ratnasamy, P., Srinivas, D., Satyanarayana, C.V.V., Manikandan, P., Kumaran, R.S., Sachin, M., and Shetti, V.N., *J. Catal.*, 2004, vol. 221, p. 455.
12. Ismailov, E.G., Maksimov, N.G., Anufrienko, V.F., and Sokolovskii, V.D., *React. Kinet. Catal. Lett.*, 1977, vol. 7, no. 1, p. 99.
13. Il'ichev, A.N., Kuli-zade, A.M., and Korchak, V.N., *Kinet. Katal.*, 2005, vol. 46, no. 3, p. 423 [*Kinet. Catal.* (Engl. Transl.), vol. 46, no. 3, p. 396].
14. Tret'yakov, I.I., Shub, B.R., and Sklyarov, A.V., *Zh. Fiz. Khim.,* 1970, vol. 44, p. 2112.
15. *Handbuch der preparativen anorganischen Chemie,* von Brauer, G., Ed., Stuttgart: Ferdinand Enke, 1981.
16. Kucherov, A.V. and Slinkin, A.A., *Usp. Khim.*, 1992, vol. 61, no. 9, p. 1687.
17. Il'ichev, A.N., Ukharskii, A.A., and Matyshak, V.A., *Kinet. Katal.*, 1995, vol. 35, no. 2, p. 268.
18. Martinez-Arias, A., Fernandez-Garcia, M., Soria, J., and Conesa, J., *J. Catal.*, 1999, vol. 182, p. 367.
19. Soria, J., Martinez-Arias, A., and Conesa, J., *J. Chem. Soc., Faraday Trans.*, 1995, vol. 91, no. 11, p. 1669.
20. Il'ichev, A.N., Shibanova, M.D., Ukharskii, A.A., Kulizade, A.M., and Korchak, V.N., *Kinet. Katal.*, 2005, vol. 46, no. 3, p. 414 [*Kinet. Catal.* (Engl. Transl.), vol. 46, no. 3, p. 387].
21. Luo, M.-F., Zhong, Y.-J., Yuan, X.-X., and Zheng, X.-M., *Appl. Catal., A,* 1997, vol. 162, p. 121.
22. Sokolovskii, V.D., Boreskov, G.K., Davydov, A.A., Gundrizer, T.A., et al., *Dokl. Akad. Nauk SSSR*, 1974, vol. 216, no. 3, p. 599.
23. Kislyuk, M.U. and Rozanov, V.V., *Kinet. Katal.,* 1995, vol. 36, no. 1, p. 89.